Hindawi Publishing Corporation
International Journal of Photoenergy
Volume 2012, Article ID 976389, 9 pages
doi:10.1155/2012/976389

Research Article

Facile Synthesis and Photocatalytic Property of Titania/Carbon Composite Hollow Microspheres with Bimodal Mesoporous Shells

Guohong Wang,[1,2] Bei Cheng,[2] Jun Zhang,[2] Lin Xu,[1] and Tingting Yin[1]

[1] *College of Chemistry and Environmental Engineering, Hubei Normal University, Huangshi, Hubei, 435002, China*
[2] *State Key Laboratory of Advanced Technology for Material Synthesis and Processing, Wuhan University of Technology, Luoshi Road No. 122, Wuhan 430070, China*

Correspondence should be addressed to Guohong Wang, wanggh2003@163.com

Received 14 September 2011; Accepted 14 November 2011

Academic Editor: Gongxuan Lu

Titania/carbon composite hollow microspheres with bimodal mesoporous shells are one-pot fabricated by hydrothermal treatment of the acidic $(NH_4)_2TiF_6$ aqueous solution in the presence of glucose at 180°C for 24 h and then calcined at 450°C. The as-prepared samples were characterized by XRD, SEM, TEM, HRTEM, UV-visible spectroscopy, and nitrogen adsorption-desorption isotherms. The photocatalytic activity of the as-prepared samples was evaluated by daylight-induced photocatalytic decolorization of methyl orange aqueous solution at ambient temperature. The effects of calcination time on the morphology, phase structure, crystallite size, specific surface area, pore structures, and photocatalytic activity of the microspheres were investigated. The results indicated that the as-obtained TiO_2/C composite hollow spheres generally exhibit bimodal mesopore size distribution with their peak intra-aggregated mesopore size in the range of 2.3–4.5 nm and peak interaggregated mesopore size in the range of 5.7–12.7 nm, depending on specific calcination time. The daylight-induced photoactivity of as-obtained hollow TiO_2/C microspheres generally exceeds that of Degussa P25. The influences of calcination time on the photoactivity are discussed in terms of carbon content, phase structures, and pore structures.

1. Introduction

Photocatalytic degradation of organic compounds for the purpose of purifying water or wastewater from industries and households has attracted great attention in the past decade [1–7]. Among various oxide semiconductor photocatalysts, titania is a very important photocatalyst due to its biological and chemical inertness, strong oxidizing power, nontoxicity, and long-term stability against photo and chemical corrosion. In order to commercialize this treatment technique, it is of great importance to improve the preparative methods of titania, because the morphology, microstructures, and photocatalytic activity of TiO_2 are significantly influenced by the preparative conditions and methods [8–11].

The fabrication of TiO_2 hollow structures attracts special attention due to their low density, high surface area, good surface permeability and larger light-harvesting capacities [9]. Especially, micro- or nanometer scale TiO_2 hollow spheres with controllable structure, composition, and properties have shown a promising perspective in many fields such as catalysts, adsorbents, sensors, light fillers, and chemical reactors [12–16]. While hollow TiO_2 structures have been synthesized without the assistance of templates by the spray-drying technique and via Ostwald ripening and chemically induced self-transformation [17–20], the templating method has been most frequently applied for the synthesis of hollow TiO_2 structures with tailored properties. For example, Hard templates (e.g., polymer latex, carbon, and anodic aluminium oxide templates) and soft

templates (e.g., supermolecules, ionic liquids, surfactant, and organogel) have been extensively employed to produce TiO_2 hollow structures either by controlled surface precipitation of inorganic molecule precursors or by direct surface reactions utilizing specific functional groups [21–27]. Very recently, a general method for the synthesis of metal oxide hollow spheres has been developed using carbonaceous polysaccharide microspheres prepared from saccharide solution as templates by Sun and coworkers and Titirici and coworkers [28, 29].

Carbon materials (e.g., amorphous carbon, activated carbon, and graphite) have attracted considerable attention due to their widespread applications as absorbents, catalyst supports, and nanocomposites [30]. Carbon is chemically inert at low temperature and a suitable support for titanium dioxide photocatalysts. Various studies have demonstrated that titanium/carbon composite photocatalysts can result in a synergistic effect of both adsorption and photocatalysis and can dramatically improve the daylight-induced photocatalytic activity of titania for different modal organic components [30–37].

However, preparation of well-crystallized titanium/carbon composite hollow microspheres with high daylight-induced photocatalytic activity keeps still a great challenge. In this study, titanium/carbon composite hollow microspheres with bimodal mesoporous shell are one-pot fabricated according to the method reported by Titirici and coworkers [29] and their visible light photocatalytic activity is investigated.

2. Experimental Section

2.1. Sample Preparation. All chemicals used in this study were reagentgrade without further purification. Distilled water was used in all experiment. $(NH_4)_2TiF_6$ was used as a titanium source. In a typical synthesis, 15 g (75.5 mmol) of glucose and 3.0 g (15.1 mmol) of $(NH4)_2TiF_6$ were dissolved in 80 and 40 mL of distilled water under stirring, respectively. The above two solutions were mixed and the pH of the mixed solutions was adjusted to ca. 3 using 1 M HCl or NaOH aqueous solutions. Then the reaction solution was transferred into a 200 mL Teflon-lined stainless steel autoclave, followed by hydrothermal treatment of the mixture at 180°C for 24 h. After hydrothermal reaction, the black or puce precipitates were centrifuged and then washed with distilled water and absolute alcohol for 5 times. The washed precipitates were dried in a vacuum oven at 60°C for 8 h. Finally, the dried mixtures were calcined in air at 450°C for 0.5–4.0 h, the TiO_2/C composites, with the color from black to grey when the calcined time was increased, were obtained. The abbreviations of TiO_2/C composites with different calcined time are shown in Tables 1 and 2.

2.2. Characterization. The carbon content of the composite catalysts was monitored using a DTA-TG instrument (Netzsch STA 449 C) in airflow of 100 mL min^{-1} at a heating rate of 10°C min^{-1} from room temperature to 900°C. The X-ray diffraction (XRD) patterns obtained on an X-ray diffractometer (type HZG41B-PC) using Cu Kα irradiation at a scan rate of 0.05° $2\theta\,s^{-1}$ were used to determine the identity of any phase present and their crystallite size. The accelerating voltage and the applied current were 15 kV and 20 mA, respectively. The phase composition of TiO_2 can be calculated from the integrated intensities of anatase (101), rutile (110), and brookite (121) peaks. If a sample contained anatase and rutile two phases, the mass fraction of rutile could be calculated according to the following equation (1) [38].

$$W_R = \frac{A_R}{0.886A_A + A_R}, \tag{1}$$

where A_A and A_R represent the integrated intensity of the anatase (101) and rutile (110) peaks, respectively. The average crystallite sizes of anatase and rutiles were determined according to the Scherrer equation using the FWHM data of each phase after correcting the instrumental broadening [38]. Morphology observation was performed on a JSM-5610LV scanning electron microscope (SEM, JEOL, Japan). Crystallite sizes and shapes were observed using transmission electron microscopy (TEM) and high-resolution transmission electron microscopy (HRTEM) (JEOL-2010F at 200 kV). The samples for TEM observation were prepared by dispersing the TiO_2 powders in an absolute ethanol solution under ultrasonic irradiation; the dispersion was then dropped on carbon-copper grids. The Brunauer-Emmett-Teller (BET) surface area (S_{BET}) of the powders was analyzed by nitrogen adsorption in a Micromeritics ASAP 2020 nitrogen adsorption apparatus (USA). All the samples were degassed at 180°C prior to nitrogen adsorption measurements. The BET surface area was determined by multipoint BET method using the adsorption data in the relative pressure (P/P_0) range 0.05 ~ 0.3. Desorption isotherm was used to determine the pore size distribution via the Barret-Joyner-Halender (BJH) method, assuming a cylindrical pore modal [39–41]. The nitrogen adsorption volume at the relative pressure (P/P_0) of 0.994 was used to determine the pore volume and average pore size. UV-visible diffuse reflectance spectra of as-prepared TiO_2 powders were obtained for the dry-pressed disk samples using a UV-visible spectrophotometer (UV2550, Shimadzu, Japan). $BaSO_4$ was used as a reflectance standard in the UV-visible diffuse reflectance experiment. The morphologies of TiO_2 powders were observed using scanning electron microscopy (SEM) (type JSM-5610LV, Japan) with an acceleration voltage of 20 kV.

2.3. Measurement of Photocatalytic Activity. The evaluation of photocatalytic activity of the prepared samples for the photocatalytic decolorization of methyl orange aqueous solution was performed at ambient temperature, as reported in our previous studies [42]. Experiments were as follows: 0.04 g of the prepared powders were dispersed in a 20 mL of methyl orange aqueous solution with a concentration of 3.1×10^{-5} mol L^{-1} in a dish (with a diameter of ca. 7.0 cm). The solution was allowed to reach an adsorption-desorption equilibrium among the photocatalyst, methyl orange, and

Table 1: Effects of calcination time on phase structure, phase content, and average crystallite sizes of TiO_2/C composite microspheres at 450°C.

Time (h)	Material abbreviations	Carbon mass ratio in composites[a] (wt.%)	Anatase		Rutile	
			Crystalline Size[b] (nm)	Content[c] (%)	Crystalline Size[b] (nm)	Content[c] (%)
0.5	TiO_2-0.5	32.9	11 (1.0)	86.2	36	13.2
1	TiO_2-1	8.2	17 (1.27)	83.5	41	16.5
2	TiO_2-2	5.0	18 (1.39)	82.5	58	17.5
4	TiO_2-4	1.9	21 (1.47)	80.6	68	18.4

[a]Estimated from the data of TGA-DSC measurement. [b]Average crystalline size of TiO_2 was determined by XRD using Scherrer equation. Relative anatase crystallinity: the relative intensity of the diffraction peak from the anatase (101) plane (indicated in parentheses, reference = sample calcined at 450°C for 0.5 h). [c]Determined by XRD method.

Table 2: Effects of calcination time on surface areas and pore parameters of TiO_2/C composite microspheres at 450°C.

Time (h)	Material abbreviations	S_{BET}[a] (m^2/g)	Pore volume[b] (cm^3/g)	Average pore Size[b] (nm)	Porosity[c] (%)
0.5	TiO_2/C-0.5	210.5	0.129	2.4	33.5
1	TiO_2/C-1	55.3	0.076	5.5	22.8
2	TiO_2/C-2	46.4	0.073	6.3	22.2
4	TiO_2/C-4	20.8	0.044	8.5	14.6

[a]The BET surface area was determined by multipoint BET method using the adsorption data in P/P_0 range from 0.05 to 0.3. [b]Pore volume and average pore size were determined by nitrogen adsorption volume at $P/P_0 = 0.994$. [c]The porosity is estimated from the pore volume determined using the desorption data at $P/P_0 = 0.994$.

water before daylight irradiation. An 18-W daylight lamp (3 cm above the dish) was used as a light source. The integrated daylight intensity was 0.46 ± 0.01 mW/cm^2, as measured by a UV radiometer (made in the photoelectric instrument factory of Beijing Normal University) with the peak intensity of 420 nm. After visible-light irradiation for 60 min, the reaction solution was filtrated, and the concentration of methyl orange aqueous solution was determined by a UV-visible spectrophotometer (UV-2550, SHIMADZU, Japan). As for the methyl orange aqueous solution with low concentration, its photocatalytic decolorization is a pseudo-first-order reaction and its kinetics may be expressed as $\ln(c_0/c) = kt$, where k is the apparent rate constant, and c_0 and c are the adsorption-desorption equilibrium and reaction concentrations of methyl orange, respectively. Each set of photocatalytic measurements were repeated for three times, and the experimental error was found to be within ±5%.

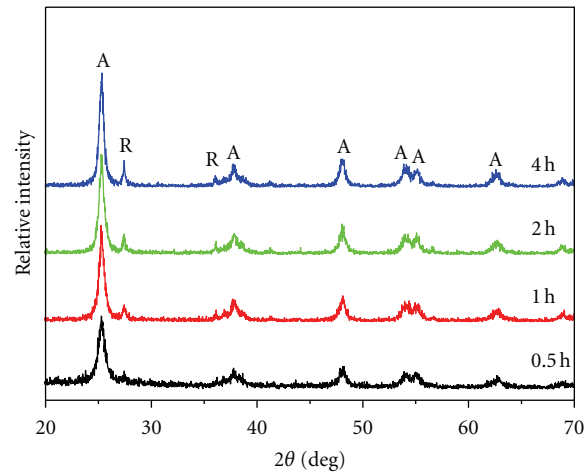

Figure 1: XRD patterns of TiO_2/C composite hollow spheres after calcination at 450°C for 0.5 (a), 1 (b), 2 (c), and 4 h (d).

3. Results and Discussion

3.1. Crystal Structure. Figure 1 shows the XRD pattern of the composites catalysts prepared at 450°C for different calcined time. The phase content, crystal size, and relative anatase crystallinity of TiO_2/C samples are shown in Table 1. At 450°C for 0.5 h, anatase and rutile phases appear, and their mass percentages are 86.2% and 13.8%, respectively. With increasing calcined time, crystallite size, relative anatase crystallinity, and rutile content increases gradually. This may be ascribed to the fact that the longer calcined time enhance grain growth and favor the phase transformation of anatase to rutile. On the other hand, with increasing calcined time from 0.5 to 4 h, the carbon content of TiO_2/C samples changes from 32.9 to 1.9%. The presence of carbon layer may suppress the phase transformation of anatase to rutile to a certain extent. Similar results were reported by Shanmugam et al. and Tsumurae al. [33, 43]. The carbon layers are acting as barriers for phase transformation of anatase to rutile.

3.2. SEM and TEM Studies. SEM and TEM were used to characterize the morphology and crystal structure of the as-prepared samples. Calcination of the TiO_2/C composites in air resulted in the formation of hollow TiO_2/C

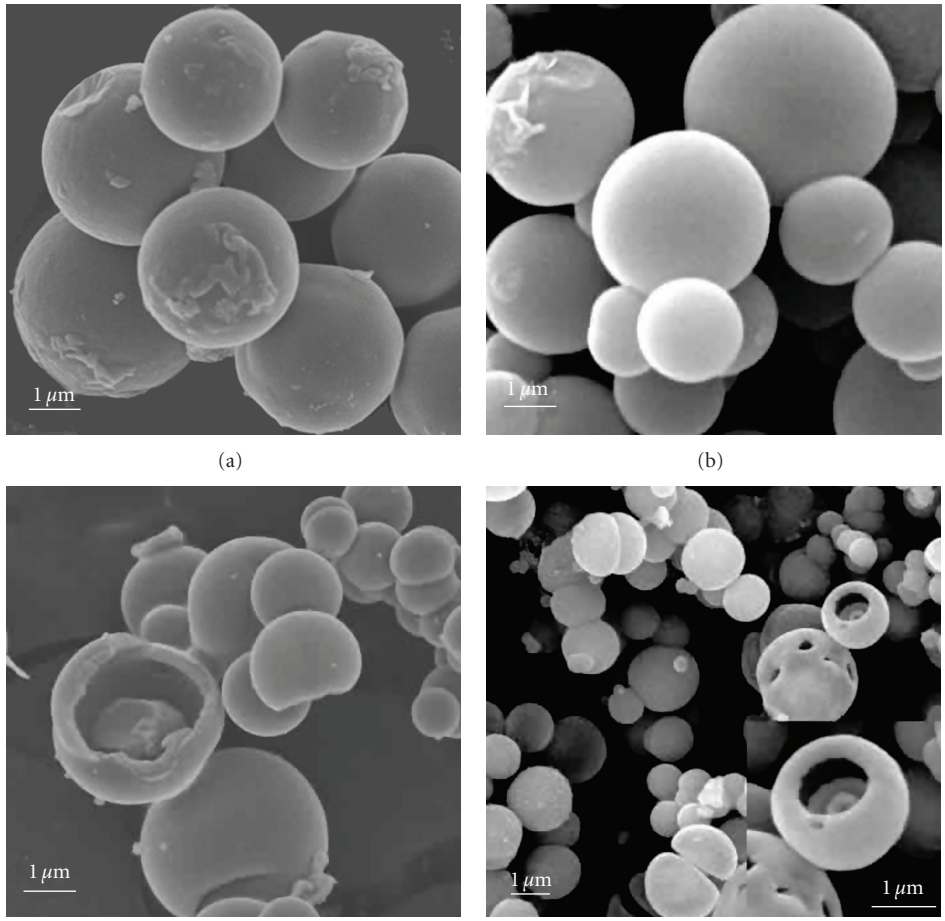

Figure 2: SEM image of the TiO_2/C composite hollow spheres calcined at 450°C for 0.5 (a), 1 (b), 2 (c), and 4 h (d).

microspheres. Figure 2 displays the SEM images of hollow TiO_2/C microspheres obtained after hydrothermal reaction and calcination in air at 450°C for different time. It can be seen from Figure 2(a) that after calcination for 0.5 h, the microspheres with surface wrinkles have a uniform diameter of ca. 4 μm. It is interesting to note that with increasing calcination time, the diameter of microspheres decrease drastically probably due to a large amount of carbon removed during calcination, resulting in drastic shrinkage of corresponding hollow spheres. At 400°C for above 2 h, the samples are composed of hollow spheres with a diameter range from 0.5 to 2.0 μm and cavities are occasionally found in some broken microspheres with a shell thickness ~400 nm (Figure 2(c) and inset in Figure 2(d)).

The morphology and microstructures of TiO_2/C hollow spheres are further investigated by TEM analysis. Figure 3(a) shows a typical TEM image of the samples calcined at 450°C for 2 h. There is a strong contrast difference observed for all microspheres with dark edge and bright center, clearly confirming their hollow structures. Further observation indicates that the prepared hollow microspheres appear unique sphere-in-sphere superstructures. Li and coworkers reported the similar sphere-in-sphere superstructures prepared solvothermally in glycerol, alcohol, and ethyl ether, which allow multireflections of electromagnetic waves, such as ultraviolet and visible light, within their interior cavities, endowing these spheres with greatly enhanced properties [44]. Figure 3(b) presents a typical HRTEM lattice image of the TiO_2 nanoparticles in the shell of TiO_2/C hollow microspheres. The selected area electron diffraction (SAED) patterns (inset in Figure 3(b)) reveal the polycrystalline nature of the anatase and rutile phases for the TiO_2/C hollow microspheres. By measuring the lattice fringes, the resolved interplanar distances are ca. 0.35 and 0.33 nm, corresponding to the (101) planes of anatase and the (110) planes of rutile, respectively. This further confirms the mixed biphase structures of hollow microspheres.

3.3. Pore Structure and BET Surface Areas. Figure 4 shows the nitrogen adsorption-desorption isotherms of the TiO_2/C composite hollow spheres calcined at 450°C for 0.5–4 h. It can be seen that all the samples show a type IV isotherm with two hysteresis loops. The shapes of two hysteresis loops are different from each other. At low relative pressures between

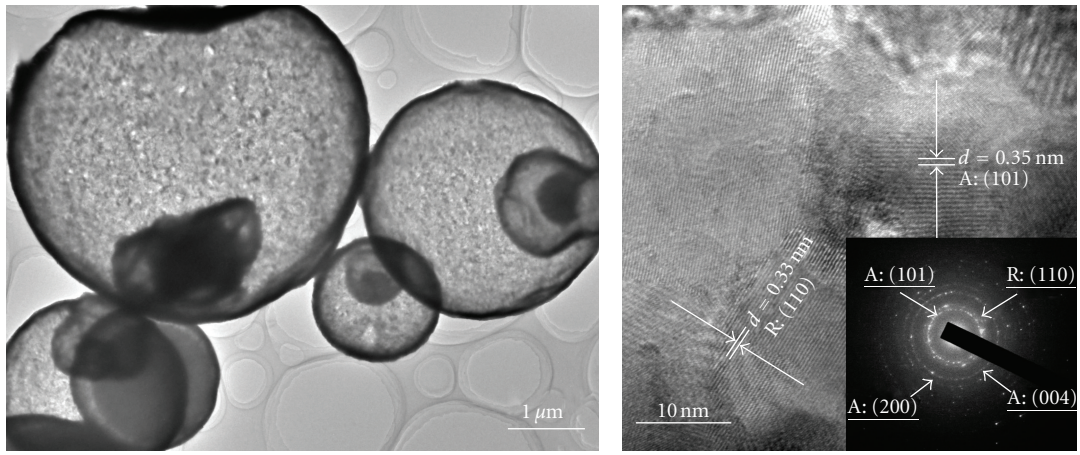

(a) (b)

Figure 3: TEM (a) and corresponding HRTEM (b) images of the TiO_2/C composite hollow spheres calcined at 450°C for 2 h.

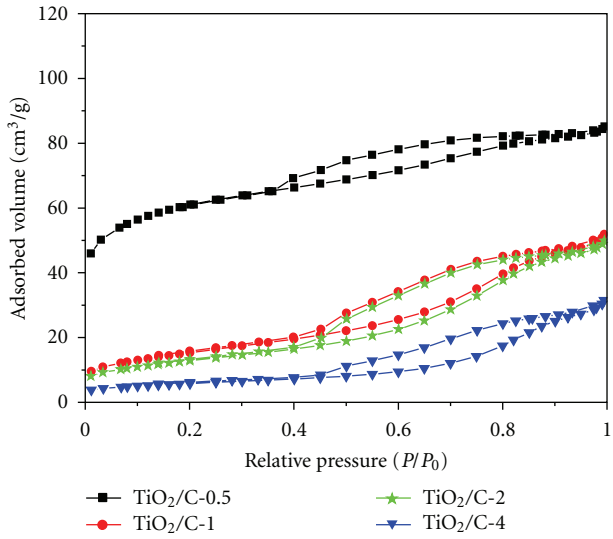

Figure 4: Nitrogen adsorption-desorption isotherms of the TiO_2/C hollow spheres calcined at 450°C for 0.5–4 h.

0.4 and 0.8, the hysteresis loops are of type H2, which can be observed in the pores with narrow necks and wider bodies (ink-bottle pores) [45, 46]. However, at high relative pressures between 0.8 and 1.0, the shape of the hysteresis loop is of a type H3, associated with plate-like particles giving rise to narrow slit-shaped pores [39, 46]. Further observation indicates that with increasing calcination time, the hysteresis loops shifted to a higher relative pressure region. The isotherms of the TiO_2/C composites prepared at 450°C for 0.4–4 h having two hysteresis loops indicate bimodal pore-size distributions in the mesoporous regions existed in the shells.

Figure 5 shows the corresponding pore-size distributions of the TiO_2/C composite hollow spheres calcined at 450°C for 0.5–4 h. All samples show bimodal pore-size distributions, consisting of finer intra-aggregated pores and larger interaggregated pores. For example, the sample calcined at 450°C for 0.5 h has small mesopores (peak pore: ca. 2.3 nm) and larger mesopores (peak pore: ca. 5.8 nm), which are related to finer aggregated pore formed between small anatase crystallites 11 nm in size, and larger aggregated pore produced by large rutile crystallites 36 nm in size (see Table 1), respectively. Further observation indicates that with increasing calcination time, the corresponding maximum peaks shift to the right, indicating the increase of pore size. There are two possible factors resulting in the increase of pore size. One is that the aggregation of greater crystallites forms bigger pores. The other is that the content of carbon in the shells decreases, which probably inserts into the pore of TiO_2 to cause the decrease in pore size. The effects of calcination time on physical properties of TiO_2/C hollow microspheres are shown in Table 2. With increasing calcination time, the BET-specific surface areas, pore volumes, and porosity steadily decrease. However, the average pore size increases. This is ascribed to the fact that increase of calcination time resulted in decrease of the carbon content in the TiO_2/C composites.

3.4. UV-Vis Spectrum. Usually, the carbon content obviously influences light absorption characteristics of TiO_2/C composites [32–35]. Figure 6 shows the UV-visible absorption spectra of the TiO_2/C composite hollow spheres calcined at 450°C for 0.5–4 h. A significant increase in the absorption at wavelengths shorter than 400 nm can be assigned to the intrinsic band gap absorption of TiO_2 [3]. It is noticeable that there is an obvious correlation between the calcination time and the UV-vis spectrum change. With increasing calcination time, the absorption in the near UV and visible-light region gradually decreases and the absorption edge of the samples shows an obvious blue shift. The differences in adsorption are attributed to the change of carbon content in the TiO_2/C composites. This clearly indicates an increase in the band gap

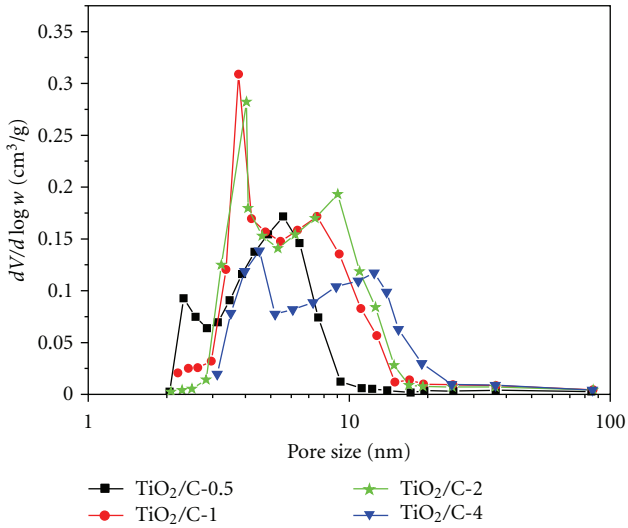

Figure 5: Pore-size distribution curves of the TiO_2/C hollow spheres calcined at 450°C for 0.5–4 h.

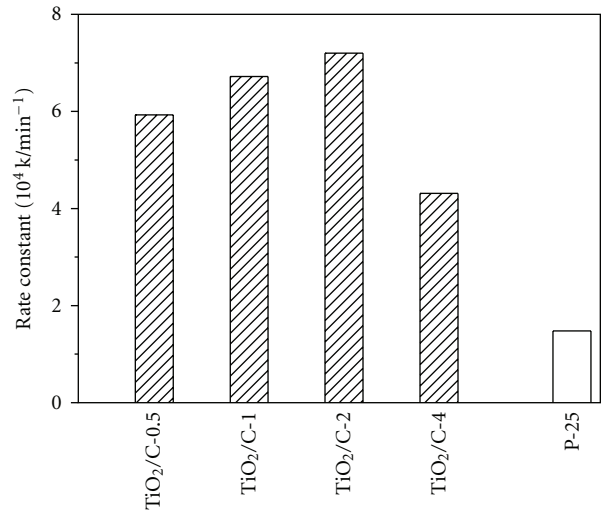

Figure 7: Effects of calcination temperatures on the apparent rate constants of the TiO_2/C composite hollow microspheres.

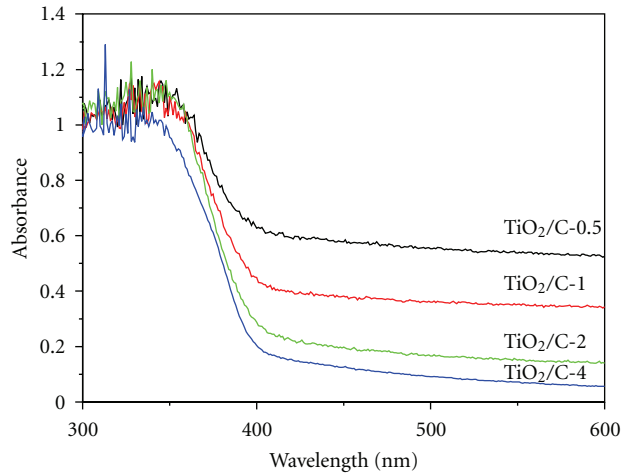

Figure 6: UV-vis spectra of TiO_2 hollow spheres calcined at 450°C for 0.5–4 h.

energy of TiO_2. Band gap energy could be estimated from Figure 6. The intercept of the tangent to the plot would give an approximation of the band gap energy for indirect band gap materials such as TiO_2 [47, 48]. The band gap energies were estimated to be about 3.05, 3.09, 3.15, and 3.20 eV for the TiO_2/C hollow spheres calcined at 450°C for 0.5, 1.0, 2.0, and 4 h, respectively. Obviously, the longer calcination time is, the bigger value of the band energies. This is due to the difference in carbon content of TiO_2/C composites [34, 49].

3.5. Photocatalytic Activity. The photocatalytic activity of the as-prepared TiO_2/C composite hollow spheres was evaluated by the daylight-induced photocatalytic decolorization of methyl orange aqueous solution at ambient temperature. For comparison, the daylight-induced photocatalytic activities of the commercial TiO_2 powder Degussa P25 (P25) were also tested. Figure 7 shows the comparisons of the apparent rate constants of P25 and the TiO_2/C composite hollow spheres at various calcination time. It can be seen that the TiO_2/C-0.5 sample has a high daylight-induced photocatalytic activity. This is due to the fact that the TiO_2/C-0.5 sample has the large carbon content of about 32.9% and surface area of 210.5 m^2/g (see Table 1). With increasing calcination time, the daylight-induced photocatalytic increases. At 450°C for 2 h, the photocatalytic activity of the TiO_2/C-2 sample reaches a maximum value, and its activity exceeds that of Degussa P25, which is recognized as an excellent photocatalyst [3, 43–45]. On the one hand, this is attributed to the former having bimodal mesoporous structures, which is more beneficial in enhancing the adsorption and desorption of reactants and products, respectively [45]. On the other hand, the high photocatalytic activity of the TiO_2/C-2 sample is due to its large surface area and high adsorption ability in the near UV and visible-light region. With further increasing calcination time, the phototcatalytic activity of the powders decreases. The highest daylight-induced phototcatalytic activity of the TiO_2-2 sample is due to the following factors.

Usually, TiO_2/C composite photocatalysts can result in a synergistic effect of both TiO_2 and carbon on the photocatalytic degradation of different modal organic components. Carbon can dramatically improve the photocatalytic activity of titania as coadsorbent due to its very high surface area. Therefore, the carbon content in the TiO_2/C composite catalysts plays an important role in its visible-light phototcatalytic activity. It can be seen from Figure 7 that the TiO_2/C-2 sample with higher carbon content shows the superior photocatalytic activity compared with the TiO_2/C-4 sample. This may be ascribed to the fact that higher carbon content results in a intense increase in absorption in the near UV and visible-light region and a red shift in the absorption edge of the TiO_2-2 sample (as shown in Figure 6), implying that the TiO_2-2 sample can be easier activated by visible

light and more photo-generated electrons and holes can be generated and participate in the photocatalytic reactions. However, adsorption of carbon is not only factor for the enhancement of the photocatalytic activity of TiO_2. For example, compared with the TiO_2-2 sample, the two TiO_2/C-0.5 and TiO_2/C-1 samples with the larger carbon content have lower daylight-induced photocatalytic activity. This result can be interpreted in two aspects. On one hand, the surplus carbon of the two TiO_2/C-0.5 and TiO_2/C-1 samples can scatter the photons in the photoreaction system [35]. On the other hand, the lower carbon content of the TiO_2/C-2 sample enables the methyl orange aqueous solution to get the active site easier and faster [33]. Therefore, the TiO_2/C-2 sample with an optimum carbon content of about 5.0% has the highest daylight-induced phototcatalytic activity.

Apart from the above carbon content, another possible understanding is that the TiO_2-1 sample possesses a relative large surface area and good anatase crystallinity (as shown in Tables 1 and 2). Usually, a large specific surface area may enhance the rate of photocatalytic degradation reactions, as a large amount of adsorbed organic molecules promote the photocatalytic reaction [50, 51]. However, the specific surface areas and crystallinity usually appear to be two conflicting intrinsic properties for TiO_2 nanoparticles [52]. The powders with a large surface area are usually associated with large amounts of crystalline defects or weak crystallization, which favor the recombination of photo-generated electrons and holes, leading to a poor photoactivity [53–55]. For example, with increasing calcination time from 0.5 to 2 h, the surface area decreases greatly, but the photocatalytic activity increases. This may be due to the increase of the relative anatase crystallinity (as shown in Table 1). So a balance between specific surface area and crystallinity is a very important factor in determining the photocatalytic activity of TiO_2 powders. According to the above results and discussion, the TiO_2/C-2 sample possesses a relative large surface area and good anatase crystallinity (as shown in Tables 1 and 2), resulting in a highest daylight-induced phototcatalytic activity.

4. Conclusions

Titania/carbon composite hollow microspheres with bimodal mesoporous shells are one-pot fabricated by hydrothermal treatment of the acidic $(NH_4)_2TiF_6$ aqueous solution in the presence of glucose at 180°C for 24 h and then calcined at 450°C for 2–4 h. Calcination time obviously influenced on the morphology, phase structure, crystallite size, specific surface area, pore structures, and daylight-induced photocatalytic activity of the as-obtained hollow microspheres. All TiO_2/C composite hollow spheres generally exhibit bimodal mesopore size distribution with their peak intra-aggregated mesopore size in the range of 2.3–4.5 nm and peak interaggregated mesopore size in the range of 5.7–12.7 nm. The TiO_2-2 sample showed the highest daylight-induced phototcatalytic activity and greatly exceeded that of Degussa P25.

Acknowledgments

This work was partially supported by NSFC (21075030, 51072154 and 51102190) and the Mid-young Scholars' Science and Technology Programs, Hubei Provincial Department of Education (Q20082202).

References

[1] M. R. Hoffmann, S. T. Martin, W. Choi, and D. W. Bahnemann, "Environmental applications of semiconductor photocatalysis," *Chemical Reviews*, vol. 95, no. 1, pp. 69–96, 1995.

[2] J. Yu, T. Ma, G. Liu, and B. Cheng, "Enhanced photocatalytic activity of bimodal mesoporous titania powders by C_{60} modification," *Dalton Transactions*, vol. 40, no. 25, pp. 6635–6644, 2011.

[3] J. G. Yu, H. G. Yu, B. Cheng, X. J. Zhao, J. C. Yu, and W. K. Ho, "The effect of calcination temperature on the surface microstructure and photocatalytic activity of TiO_2 thin films prepared by liquid phase deposition," *Journal of Physical Chemistry B*, vol. 107, no. 50, pp. 13871–13879, 2003.

[4] P. Madhusudan, J. Ran, J. Zhang, J. Yu, and G. Liu, "Novel urea assisted hydrothermal synthesis of hierarchical $BiVO_4/Bi_2O_2CO_3$ nanocomposites with enhanced visible-light photocatalytic activity," *Applied Catalysis B*, vol. 110, pp. 286–295, 2011.

[5] A. Yu, G. Q. M. Lu, J. Drennan, and I. R. Gentle, "Tubular titania nanostructures via layer-by-layer self-assembly," *Advanced Functional Materials*, vol. 17, no. 14, pp. 2600–2605, 2007.

[6] M. Andersson, L. Österlund, S. Ljungström, and A. Palmqvist, "Preparation of nanosize anatase and rutile TiO_2 by hydrothermal treatment of microemulsions and their activity for photocatalytic wet oxidation of phenol," *Journal of Physical Chemistry B*, vol. 106, no. 41, pp. 10674–10679, 2002.

[7] H. Yu, J. Yu, B. Cheng, and S. Liu, "Novel preparation and photocatalytic activity of one-dimensional TiO_2 hollow structures," *Nanotechnology*, vol. 18, Article ID 65604, 8 pages, 2007.

[8] J. Yu and H. Tang, "Solvothermal synthesis of novel flower-like manganese sulfide particles," *Journal of Physics and Chemistry of Solids*, vol. 69, no. 5-6, pp. 1342–1345, 2008.

[9] J. Yu, S. Liu, and H. Yu, "Microstructures and photoactivity of mesoporous anatase hollow microspheres fabricated by fluoride-mediated self-transformation," *Journal of Catalysis*, vol. 249, no. 1, pp. 59–66, 2007.

[10] J. Yu, G. Wang, B. Cheng, and M. Zhou, "Effects of hydrothermal temperature and time on the photocatalytic activity and microstructures of bimodal mesoporous TiO_2 powders," *Applied Catalysis B*, vol. 69, no. 3-4, pp. 171–180, 2007.

[11] G. Wang, "Hydrothermal synthesis and photocatalytic activity of nanocrystalline TiO_2 powders in ethanol-water mixed solutions," *Journal of Molecular Catalysis A*, vol. 274, no. 1-2, pp. 185–191, 2007.

[12] Z. Zhong, Y. Yin, B. Gates, and Y. Xia, "Preparation of mesoscale hollow spheres of TiO_2 and SnO_2 by templating against crystalline arrays of polystyrene beads," *Advanced Materials*, vol. 12, no. 3, pp. 206–209, 2000.

[13] Y. Z. Zhu, Y. L. Cao, Z. H. Li, J. Ding, J. S. Liu, and Y. B. Chi, "Synthesis and photonic band calculations of NCP face-centered cubic photonic crystals of TiO_2 hollow spheres,"

Journal of Colloid and Interface Science, vol. 306, no. 1, pp. 133–136, 2007.

[14] D. Wang, C. Song, Y. Lin, and Z. Hu, "Preparation and characterization of TiO_2 hollow spheres," *Materials Letters*, vol. 60, no. 1, pp. 77–80, 2006.

[15] J. Yu and J. Zhang, "A simple template-free approach to TiO_2 hollow spheres with enhanced photocatalytic activity," *Dalton Transactions*, vol. 39, no. 25, pp. 5860–5867, 2010.

[16] V. Jokanović, B. Jokanović, J. Nedeljković, and O. Milošević, "Modeling of nanostructured TiO_2 spheres obtained by ultrasonic spray pyrolysis," *Colloids and Surfaces A*, vol. 249, no. 1–3, pp. 111–113, 2004.

[17] S. Liu, J. Yu, and M. Jaroniec, "Tunable photocatalytic selectivity of hollow TiO_2 microspheres composed of anatase polyhedra with exposed 001 facets," *Journal of the American Chemical Society*, vol. 132, no. 34, pp. 11914–11916, 2010.

[18] J. Yu, Q. Xiang, J. Ran, and S. Mann, "One-step hydrothermal fabrication and photocatalytic activity of surface-fluorinated TiO_2 hollow microspheres and tabular anatase single microcrystals with high-energy facets," *Crystal Engineering communication*, vol. 12, no. 3, pp. 872–879, 2010.

[19] J. Li and C. Z. Hua, "Size tuning, functionalization, and reactivation of Au in TiO_2 nanoreactors," *Angewandte Chemie*, vol. 44, no. 28, pp. 4342–4345, 2005.

[20] J. Yu, H. Guo, S. A. Davis, and S. Mann, "Fabrication of hollow inorganic microspheres by chemically induced self-transformation," *Advanced Functional Materials*, vol. 16, no. 15, pp. 2035–2041, 2006.

[21] T. Peng, A. Hasegawa, J. Qiu, and K. Hirao, "Fabrication of titania tubules with high surface area and well-developed mesostructural walls by surfactant-mediated templating method," *Chemistry of Materials*, vol. 15, no. 10, pp. 2011–2016, 2003.

[22] Q. Peng, S. Xu, Z. Zhuang, X. Wang, and Y. Li, "A general chemical conversion method to various semiconductor hollow structures," *Small*, vol. 1, no. 2, pp. 216–221, 2005.

[23] S. Kobayashi, K. Hanabusa, N. Hamasaki, M. Kimura, H. Shirai, and S. Shinkai, "Preparation of TiO_2 hollow-fibers using supramolecular assemblies," *Chemistry of Materials*, vol. 12, no. 6, pp. 1523–1525, 2000.

[24] T. Nakashima and N. Kimizuka, "Interfacial synthesis of hollow TiO_2 microspheres in ionic liquids," *Journal of the American Chemical Society*, vol. 125, no. 21, pp. 6386–6387, 2003.

[25] T. Z. Ren, Z. Y. Yuan, and B. L. Su, "Surfactant-assisted preparation of hollow microspheres of mesoporous TiO_2," *Chemical Physics Letters*, vol. 374, no. 1-2, pp. 170–175, 2003.

[26] J. H. Jung, H. Kobayashi, K. J. C. Van Bommel, S. Shinkai, and T. Shimizu, "Creation of novel helical ribbon and double -layered nanotube TiO_2 structures using an organogel template," *Chemistry of Materials*, vol. 14, no. 4, pp. 1445–1447, 2002.

[27] S. M. Liu, L. M. Gan, L. H. Liu, W. D. Zhang, and H. C. Zeng, "Synthesis of single-crystalline TiO_2 nanotubes," *Chemistry of Materials*, vol. 14, no. 3, pp. 1391–1397, 2002.

[28] X. Sun, J. Liu, and Y. Li, "Use of carbonaceous polysaccharide microspheres as templates for fabricating metal oxide hollow spheres," *Chemistry*, vol. 12, no. 7, pp. 2039–2047, 2006.

[29] M. M. Titirici, M. Antonietti, and A. Thomas, "A generalized synthesis of metal oxide hollow spheres using a hydrothermal approach," *Chemistry of Materials*, vol. 18, no. 16, pp. 3808–3812, 2006.

[30] D. Zhang, D. Yang, H. Zhang, C. Lu, and L. Qi, "Synthesis and photocatalytic properties of hollow microparticles of titania and titania/carbon composites templated by sephadex G-100," *Chemistry of Materials*, vol. 18, no. 15, pp. 3477–3485, 2006.

[31] Y. Tao, S. Schwartz, C. Y. Wu, and D. W. Mazyck, "Development of a TiO_2/AC composite photocatalyst by dry impregnation for the treatment of methanol in humid airstreams," *Industrial and Engineering Chemistry Research*, vol. 44, no. 19, pp. 7366–7372, 2005.

[32] W.-C. Oh and M.-L. Chen, "The improved photocatalytic properties of methylene blue for V_2O_3/CNT/TiO_2 composite under visible light," *International Journal of Photoenergy*, vol. 2010, Article ID 264831, 12 pages, 2010.

[33] S. Shanmugam, A. Gabashvili, D. S. Jacob, J. C. Yu, and A. Gedanken, "Synthesis and characterization of TiO_2@C core-shell composite nanoparticles and evaluation of their photocatalytic activities," *Chemistry of Materials*, vol. 18, no. 9, pp. 2275–2282, 2006.

[34] J. Yu, T. Ma, and S. Liu, "Enhanced photocatalytic activity of mesoporous TiO_2 aggregates by embedding carbon nanotubes as electron-transfer channel," *Physical Chemistry Chemical Physics*, vol. 13, no. 8, pp. 3491–3501, 2011.

[35] W. Wang, P. Serp, P. Kalck, and J. L. Faria, "Visible light photodegradation of phenol on MWNT-TiO_2 composite catalysts prepared by a modified sol-gel method," *Journal of Molecular Catalysis A*, vol. 235, no. 1-2, pp. 194–199, 2005.

[36] Q. Xiang, J. Yu, and M. Jaroniec, "Enhanced photocatalytic H_2-production activity of graphene-modified titania nanosheets," *Nanoscale*, vol. 3, no. 9, pp. 3670–3678, 2011.

[37] Y. Tao, C. Y. Wu, and D. W. Mazyck, "Microwave-assisted preparation of TiO_2/activated carbon composite photocatalyst for removal of methanol in humid air streams," *Industrial and Engineering Chemistry Research*, vol. 45, no. 14, pp. 5110–5116, 2006.

[38] J. Yu, J. C. Yu, M. K. P. Leung et al., "Effects of acidic and basic hydrolysis catalysts on the photocatalytic activity and microstructures of bimodal mesoporous titania," *Journal of Catalysis*, vol. 217, no. 1, pp. 69–78, 2003.

[39] K. S. W. Sing, D. H. Everett, and R. A. W. Haul, "Reporting physisorption data for gas/solid systems with special reference to the determination of surface area and porosity," *Pure and Applied Chemistry*, vol. 57, no. 4, pp. 603–619, 1985.

[40] S. J. Gregg and K. S. W. Sing, *Adsorption, Surface Area and Porosity*, Academic Press, London, UK, 1982.

[41] E. P. Barrett, L. G. Joyner, and P. P. Halenda, "The determination of pore volume and area distributions in porous substances. I. Computations from nitrogen isotherms," *Journal of the American Chemical Society*, vol. 73, no. 1, pp. 373–380, 1951.

[42] H. Yu, J. Yu, S. Liu, and S. Mann, "Template-free hydrothermal synthesis of CuO/Cu_2O composite hollow microspheres," *Chemistry of Materials*, vol. 19, no. 17, pp. 4327–4334, 2007.

[43] T. Tsumura, N. Kojitani, I. Izumi, N. Iwashita, M. Toyoda, and M. Inagaki, "Carbon coating of anatase-type TiO_2 and photoactivity," *Journal of Materials Chemistry*, vol. 12, no. 5, pp. 1391–1396, 2002.

[44] H. Li, Z. Bian, J. Zhu et al., "Mesoporous titania spheres with tunable chamber stucture and enhanced photocatalytic activity," *Journal of the American Chemical Society*, vol. 129, no. 27, pp. 8406–8407, 2007.

[45] J. Yu, J. C. Yu, W. Ho et al., "Effects of alcohol content and calcination temperature on the textural properties of bimodally mesoporous titania," *Applied Catalysis A*, vol. 255, no. 2, pp. 309–320, 2003.

[46] J. G. Yu, J. C. Yu, B. Cheng, S. K. Hark, and K. Iu, "The effect of F^- doping and temperature on the structural and textural evolution of mesoporous TiO_2 powders," *Journal of Solid State Chemistry*, vol. 174, no. 2, pp. 372–380, 2003.

[47] K. N. P. Kumar, J. Kumar, and K. Keizer, "Effect of peptization on densification and phase-transformation behavior of sol-gel-derived nanostructured titania," *Journal of the American Ceramic Society*, vol. 77, no. 5, pp. 1396–1400, 1994.

[48] N. Serpone, D. Lawless, and R. Khairutdinov, "Size effects on the photophysical properties of colloidal anatase TiO_2 particles: size quantization or direct transitions in this indirect semiconductor?" *Journal of Physical Chemistry*, vol. 99, no. 45, pp. 16646–16654, 1995.

[49] J. Yu, M. Zhou, B. Cheng, and X. Zhao, "Preparation, characterization and photocatalytic activity of in situ N,S-codoped TiO_2 powders," *Journal of Molecular Catalysis A*, vol. 246, no. 1-2, pp. 176–184, 2006.

[50] J. Yu, M. Zhou, B. Cheng, H. Yu, and X. Zhao, "Ultrasonic preparation of mesoporous titanium dioxide nanocrystalline photocatalysts and evaluation of photocatalytic activity," *Journal of Molecular Catalysis A*, vol. 227, no. 1-2, pp. 75–80, 2005.

[51] M. Zhou, J. Yu, B. Cheng, and H. Yu, "Preparation and photocatalytic activity of Fe-doped mesoporous titanium dioxide nanocrystalline photocatalysts," *Materials Chemistry and Physics*, vol. 93, no. 1, pp. 159–163, 2005.

[52] G. Liu, Z. Chen, C. Dong et al., "Visible light photocatalyst: iodine-doped mesoporous titania with a bicrystalline framework," *Journal of Physical Chemistry B*, vol. 110, no. 42, pp. 20823–20828, 2006.

[53] O. Carp, C. L. Huisman, and A. Reller, "Photoinduced reactivity of titanium dioxide," *Progress in Solid State Chemistry*, vol. 32, no. 1-2, pp. 33–177, 2004.

[54] K. Tanaka, M. F. V. Capule, and T. Hisanaga, "Effect of crystallinity of TiO_2 on its photocatalytic action," *Chemical Physics Letters*, vol. 187, no. 1-2, pp. 73–76, 1991.

[55] B. Ohtani, Y. Ogawa, and S. I. Nishimoto, "Photocatalytic activity of amorphous-anatase mixture of titanium(IV) oxide particles suspended in aqueous solutions," *Journal of Physical Chemistry B*, vol. 101, no. 19, pp. 3746–3752, 1997.